Journal of Advanced Research 22 (2020) 105–118

Contents lists available at ScienceDirect

Journal of Advanced Research

journal homepage: www.elsevier.com/locate/jare

Original Article

Thermotolerance and plasticity of camel somatic cells exposed to acute and chronic heat stress

Islam M. Saadeldin [a,c,*,1], Ayman Abdel-Aziz Swelum [a,d,1], Mona Elsafadi [b], Amer Mahmood [b], Aya Osama [e], Hassan Shikshaky [e], Musaad Alfayez [b,g], Abdullah N. Alowaimer [a], Sameh Magdeldin [e,f,*]

[a] Department of Animal Production, College of Food and Agricultural Sciences, King Saud University, 11451 Riyadh, Saudi Arabia
[b] Stem Cell Unit, Department of Anatomy, College of Medicine, King Saud University, Riyadh, Saudi Arabia
[c] Department of Physiology, Faculty of Veterinary Medicine, Zagazig University, 44519 Zagazig, Egypt
[d] Department of Theriogenology, Faculty of Veterinary Medicine, Zagazig University, 44519 Zagazig, Egypt
[e] Proteomics and Metabolomics Unit, 57357 Children's Cancer Hospital, Cairo, Egypt
[f] Physiology Department, Faculty of Veterinary Medicine, Suez Canal University, Ismailia, Egypt
[g] Saudi Society for Camel Research, King Saud University, Saudi Arabia

HIGHLIGHTS

- The molecular explanation for the thermotolerance of camel somatic cells has been studied.
- Acute heat shock increased expression of heat shock proteins and DNA repair enzymes.
- Actin polymerization and Rho signaling were critically activated against heat shock.
- Chronic heat shock altered cell architecture, proteomics, and cytoskeletal proteins.
- TGFβ pathway was involved in morphological alterations of cells exposed to chronic heat shock.
- Proteomic changes were restored during recovery stage and cells regained normal morphology.

GRAPHICAL ABSTRACT

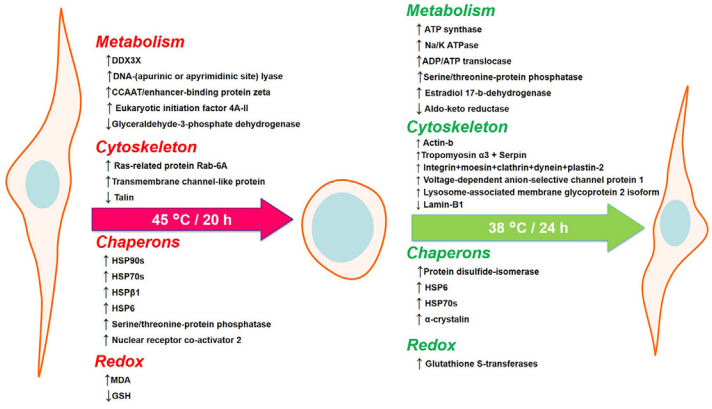

ARTICLE INFO

Article history:
Received 18 August 2019
Revised 5 November 2019
Accepted 19 November 2019
Available online 22 November 2019

Keywords:
HSPs

ABSTRACT

The Arabian camel is the largest known mammal that can survive in severe hot climatic conditions. We provide the molecular explanation for the thermotolerance of camel granulosa somatic cells after exposure to 45 °C for 2 (acute heat shock) or 20 h (chronic heat shock). The common features of the cellular responses to acute heat stress were the increase of heat shock proteins and DNA repair enzymes expression. Actin polymerization and Rho signaling were critically activated as a cellular defense against heat shock. Cells exposed to chronic heat shock showed altered cell architecture with a decrease in total detected proteins, metabolic enzymes, and cytoskeletal protein expression. Treatment with transforming

Abbreviations: CB, Cytochalasin B; GSH, reduced glutathione; HSPs, heat shock proteins; IDA, information dependent acquisition; MDA, malondialdehyde; RI, ROCK-inhibitor; ROCKs, Rho-associated protein kinases; TGFβ, transforming growth factor beta; TIC, total ion chromatography; Y-27632, ROCK-inhibitor Y-27632.

Peer review under responsibility of Cairo University.

* Corresponding authors at: Department of Animal Production, College of Food and Agricultural Sciences, King Saud University, 11451 Riyadh, Saudi Arabia (I.M. Saadeldin).
E-mail addresses: isaadeldin@ksu.edu.sa (I.M. Saadeldin), aswelum@ksu.edu.sa (A.A.-A. Swelum), melsafadi@ksu.edu.sa (M. Elsafadi), ammahmood@ksu.edu.sa (A. Mahmood), aya.osama@57357.org (A. Osama), hassan.ismail@57357.org (H. Shikshaky), alfayez@ksu.edu.sa (M. Alfayez), aowaimer@ksu.edu.sa (A.N. Alowaimer), sameh.magdeldin@57357.org (S. Magdeldin).
[1] Authors have contributed equally.

https://doi.org/10.1016/j.jare.2019.11.009
2090-1232/

ROCK
Actin
TGFβ
Proteomics
Camel
Anastasis

growth factor beta (TGFβ) pathway inhibitor SB-431542 suppressed the morphological alterations of cells exposed to chronic heat shock. Moreover, during the recovery stage at 38 °C for 24 h, proteomic changes were partially restored with an exponential increase in *HSP70* expression, and the cells restored their normal cellular morphology on the 9th day of recovery. Full proteomics data are available *via* ProteomeXchange with identifier PXD012159. The strategies of cellular defense and tolerance to both thermal conditions reflect the flexible adaptability of camel somatic cells to conserve life under extremely hot conditions.

Introduction

Increasing global warming has led to a coinciding increase in research on the key detrimental factors of heat stress (HS) affecting animal welfare, livestock production, and human health. Increased temperatures above the normal limit or prolonged exposure to extreme environmental temperatures reduces cell viability when cellular defense mechanisms are not sufficient to withstand against this stress [1].

Living organisms react to hyperthermia through up-and-down regulation of genes correlated with cell defense against the detrimental effects of cellular protein denaturation and cytoskeleton disorganization [2]. Mostly, when exposed to heat stress, cells respond by a rapid and selective increase in heat shock proteins (HSPs) synthesis and by a dramatic reorganization of various cytoskeletal networks such as microtubules, intermediate filaments, and actin microfilaments [3]. The camel (*Camelus dromedarius*) is one of the largest xeric mammals that can survive in conditions of extreme dehydration and high temperatures for extended periods of time [4]. It increases the internal body temperature (Tb) to reach 43 °C during severe hot and dry conditions and dissipates this heat with the cold subjects to lower body temperature again [5]. Comparative genomics have predicted that the adaptability of camelids to xeric life conditions is due to unique lipid metabolism and stress responses to extreme environmental conditions [6].

Extremely elevated temperatures cause damaging effects on metabolic machinery, such as inhibition of enzymes' catalytic activities, single and double-stranded DNA breaks and mutations, in addition to inhibition of DNA repair pathways [7]. Furthermore, apoptosis and necrosis may occur to somatic cells, such as Jurkat cells, at 44 °C and 46 °C, respectively [1]. Researchers have suggested that cellular responses to acute and chronic thermal stresses are different [8]. Clearly, prolonged exposure of cells to heat shock disrupted the cell morphology, and caused apoptosis, autophagy, and necrosis [9,10]. Preliminary results indicate clear resistance by camel cells, suggesting unique cellular defense mechanisms following prolonged exposure to lethal heat.

Observations showed a mutual relationship between cell survival and the induction of heat shock proteins. Cells that produce excessive heat shock proteins at high temperatures will combat both thermal and oxidative stress and sustain viability [1].

Collective evidences revealed that dying cells can recover following apoptosis and ferroptosis in a process called "anastasis" [11]. Anastasis is a term coined to outline the process of cell recovery or cellular resurrection from the brink of cell death [12].

Recently, we showed different thermotolerance capabilities between camel somatic cells and oocyte [10]. Moreover, we showed the different durability against chronic heat shock among different somatic cells of camels [13]. The impetus of the current study is to investigate the molecular mechanisms controlling thermotolerance of camel somatic cells after exposure to acute (45 °C/2 h) or chronic heat stress (45 °C/20 h), which is a lethal temperature for most of mammalian cells [1]. This study provides a paradigm for strategies of cellular thermotolerance, which can provide better explanation of the unique characteristics of camel cells.

Materials and methods

Chemicals

Chemicals and culture media were obtained from Sigma-Aldrich Corp. (St. Louis, MO, USA) unless otherwise indicated.

Granulosa cell culture

Cells were obtained from camel ovaries. Ovaries were collected after routine animal slaughter at a local abattoir in Riyadh city. There was no member of the research team involved in pre-slaughter live animal handling or in the process of slaughtering. Ovaries were then transported to the laboratory within 4 to 6 h in a warm normal saline solution (30 to 33 °C). Antral follicles (2–8 mm in diameter) contents were collected using 10 mL disposable syringe. Cumulus-oocytes complexes were excluded from the follicular fluid contents under stereomicroscope using sterilized Pasteur pipette. Primary culture of granulosa cells was performed in 4-well tissue culture dishes (Falcon, BD Biosciences, Franklin lakes, NJ, USA). The culture medium consisted of Dulbecco's modified Eagle medium (DMEM), 10% fetal bovine serum (FBS), and 1 mg/mL gentamycin. Cells were cultured at 38 °C in a humidified atmosphere of 5% CO_2 for 2 days. Culture medium was changed every 2 days until the cells reached 90% confluency. Primary culture of porcine granulosa cells were kindly provided by Dr. Goo Jang from Seoul National University, South Korea, and were handled similarly as camel granulosa cells.

Heat exposure and examination of cell viability

Cells were distributed into six 4-well dishes (viable cell count of $10.0 \pm 1.0 \times 10^4$/mL). Following the cellular attachment, culture dishes were exposed to one of the following conditions: (1) incubation at 45 °C for 2 h (acute exposure), followed by 38 °C for recovery; (2) incubation at 45 °C for 20 h (chronic exposure), followed by 38 °C for recovery. Each treatment was accompanied with a control group which was initially cultured at 38 °C. Time-lapse imaging was performed using JuLI™ Live Cell Movie analyzer (NanoEnTek Inc., Seoul, Korea). All control, heat shock and time-lapse experiments were performed using humid humidified atmosphere of 5% CO_2 (ThermoFisher Sci., Waltham, MA, USA) of For revealing the role of TGFβ pathway during the chronic heat stress, we treated the cells with TGFβ pathway inhibitor SB-431542 of dose 20 μM [14] during the exposure to 45 °C for 20 h. Following the treatments, cells were collected by trypsinization and washing in PBS, and finally suspended in 1 mL PBS. Equal amounts of cell suspension and trypan blue solution (0.4% solution in PBS) were gently

mixed, loaded into a hemocytometer and examined under a microscope at low magnification. The ratios of dead cells (blue-stained) to total cells were recorded. The experiment was repeated five times, and the values were recorded as mean ± SEM.

Measurements of oxidative stress markers (malondialdehyde and reduced glutathione)

Malondialdehyde (MDA), the lipid peroxide, and reduced glutathione (GSH) levels were measured in the conditioned medium of five replicates using colorimetric methods. For MDA, thiobarbituric acid was allowed to react with MDA in an acidic medium at 95 °C for 30 min. The absorbance of this resulting reaction was measured at a wavelength of 534 nm. GSH level measurement was based on the reduction of 5,5′ dithiobis (2-nitrobenzoic acid) by glutathione to produce a reduced yellow compound which is directly proportional to GSH concentrations. The absorbance of the resulted chromogen was measured at a wavelength of 405 nm.

Relative quantitative PCR (qPCR)

Cells (three replicates) were trypsinized, washed in PBS and collected with centrifugation at 1000 xg for 2 min. RNA was extracted from cell pellets using a total RNA extraction Kit (Intron Biotech, Seoul, Korea). RNA concentration and purity were estimated by NanoDrop 2000 spectrophotometer (Thermo Fisher). Pulsed reverse transcription (RT) was performed according to Mestdagh et al. [15] with some modifications [10]: 120 cycles of 16 °C for 2 min, 37 °C for 1 min, and 50 °C for 1 s, followed by final inactivation at 85 °C for 5 min. RT reactions were comprised of 50 ng of total RNA, and 5 μM of random hexamers in a 40 μL total reaction volume using a High-Capacity cDNA Reverse Transcription Kit (Applied Biosystems, Foster City, CA, USA). Relative quantitative real-time PCR was performed using automated thermal cycler (ViiA 7, Applied Biosystems). Reactions comprised of 100 ng of cDNA, 1 μM forward and reverse primers, and 1 × SYBR Green premix (Applied Biosystems). House-keeping gene *GAPDH* was used for normalization and the fold-change of the target transcripts were calculated through the $2^{-\Delta\Delta Ct}$ method. cDNA template-negative samples and reactions without RT resulted in no amplification in all assays. Thermal cycling conditions were 95 °C for 10 min, followed by 40 cycles of 95 °C for 10 s, 60 °C for 20 s, and 72 °C for 40 s. Details of primers used to amplify the target transcripts are listed in Supplementary Table 1.

Shotgun proteomics analysis

Preparation of cell protein lysate

Collected cells were quickly washed with cold PBS supplemented with a protease and phosphatases inhibitors (complete ultra-tablets, mini, Roche, Mannheim) to suppress any possible protease activity such as that of phosphofructokinase. Protein was extracted from the cells by combining approximately 200 μL (1×10^4) of cells with 1 mL lysis solution (8 M urea, 500 mM Tris HCl, pH 8.5) and complete ultra-protease inhibitor (Roche, Mannheim). After incubation at 37 °C for 1 h with occasional vortex, samples were centrifuged at 12,000 rpm for 20 min. Acetone was used to precipitate the lysate and was measured through the BCA method (Pierce, Rockford IL) at Å562 nm prior to digestion.

Preparation of tryptic digest

Thirty μg of cell protein lysate from each sample was subjected to digestion in solution. In brief, protein pellets were suspended in 8 M urea lysis solution and reduced with 5 mM tris(2-carboxyethyl)phosphine (TCEP) for 30 min. Alkylation of cysteine residues were performed with 10 mM iodoacetamide for 30 min in the dark. Prior to digestion with trypsin, samples were diluted to a final concentration of 2 M urea with 100 mM Tris-HCl, pH 8.5. A modified procaine trypsin (Sigma, Germany) was added at ratio of 50:1 (protein: protease mass) along with 1 mM $CaCl_2$ and incubated overnight in a thermo-shaker at 600 rpm and 37 °C for endopeptidase digestion. The digested peptide solution was acidified using 90% formic acid to a final pH of 2.0. The resultant peptide mixture was cleaned using stage tip and quantified as discussed previously [16]. Each sample was run in triplicate.

Nano-LC MS/MS analysis

Nano-LC MS/MS analysis was conducted using a TripleTOF 5600 + (AB Sciex, Canada) connected at the front end with a Eksigent nanoLC 400 autosampler with Ekspert nanoLC 425 pump. Peptides were trapped on a CHROMXP C18CL 5 μm column (10 × 0.5 mm) (Sciex, Germany) on trap and elute mode. MS and MS/MS ranges were 400–1250 *m*/*z* and 170–1500 *m*/*z*, respectively. Samples were eluted on a 55-minute linear gradient 3–40% solution (80% ACN, 0.2% formic acid). The 40 most intense ions were sequentially selected in data dependent acquisition (DDA) mode with a 2–5 charge state. Surveys of full scan MS and MS/MS spectra were estimated at resolutions of 35.000 and 15.000, respectively. External calibration was scheduled and run during sample batches to correct possible TOF deviation to ensure the analysis accuracy.

Proteomics data analysis

Mascot generic format (mgf) files were generated from raw files using a script supplied by AB Sciex. MS/MS spectra were analyzed using X Tandem in Peptide shaker (version 1.16.26) against the *Camelus* UniProtKB/TrEMBL database (462 entries) with reversed decoy sequences. The search space included all fully and semi-tryptic peptide candidates (containing up to 2 missed cleavages with at least 6 amino acids). Precursor mass and fragment mass were identified with an initial mass tolerance of 20 ppm and 10 ppm, respectively. Carbamidomethylation of cysteine (+57.02146 amu) was considered a static modification and oxidation of Methionine (+15.995), acetylation of protein N- terminal and K (+42.01 amu), and pyrrolidone from carbamidomethylation C (−17.03 amu) as variable modification. To ensure high quality results, the false discovery rate (FDR) was kept at 1% at the protein level. Final assembly of sample replicates was applied to generate final outputs for each sample and normalized spectral abundance factor (NSAF) normalization was used to compare the protein abundance as fold-change between the samples according to Gokce et al. [17]. Total ion chromatography (TIC) and Information Dependent Acquisition (IDA) were also performed for cells exposed to acute and chronic thermal stress and represented in Supplementary Figs. 1 and 2, respectively. Detailed analysis of proteomics are shown in Supplementary Excel files 1 and 2 for acute and chronic heat shock, respectively.

Cytochalasin B treatment and wound healing

Cells were randomly allocated into three treatments: cells incubated at 45 °C treated with or without 0.5 mg/ml cytochalasin B (CB), and cells were incubated at 38 °C and treated with CB for two hours. After removal of CB, cells were microscopically examined to determine the effect of CB on morphology and then were subjected to a scratch healing assay following our recent report [10]. In brief, granulosa cells from the three treatments were distributed in 35 mm dishes and cultured until confluent. The cell

monolayers were then scraped in a straight line with sterile 1000-microliter blue pipette tips to create a wound, washed with culture medium to remove debris at the edge of the scratch. Culture medium was replaced with 2 mL and the dishes were then incubated at 38 °C in humid atmosphere of 5% CO_2. Cell growth and wound healing was assessed by capturing images and measuring the mean distance between the wound edges with ImageJ 1.50i software (NIH, USA).

ROCK-inhibitor Y-27632 treatment and wound healing

Cells were randomly allocated into three treatments: cells incubated at 45 °C with or without 10 μM ROCK-inhibitor Y-27632 (RI) treatment, or incubated at 38 °C and treated with RI for two hours. After removal of RI, cells were microscopically examined and then subjected to a wound healing assay as previously described. Cell growth and wound healing were assessed as previously mentioned.

Statistical analysis

Values were presented as mean ± SEM. Cell replication values were analyzed using ANOVA. Quantitative PCR results were compared by Student T-test. Significant statistical differences were considered when $P \leq 0.05$. Normalized spectral abundance factor (NSAF) and protein expression alteration (fold changes), log values, and confidence were calculated based on spectral peak intensities generated from the mass spectrometric analysis after extracting confident protein spectra with $P < 0.05$ [18]. Results were considered as non- significant if P value was higher than earlier indicated value. Proteomics data analysis and associated illustrations were performed using R language unless otherwise stated.

Results

Impact of heat shock on camel cell morphology

Cells exposed to acute heat shock (45 °C for 2 h) retained their normal spindle shape with no other observed morphological changes (Fig. 1B). However, chronic heat shock significantly distorted the cell morphology. Cells in the control group and during the pre-exposure period were characterized by spindle shape and ovoid nuclei (Fig. 1A). Moreover, cells showed temporal morphological changes after exposure to 45 °C for 5, 10, and 20 h. Cells became polygonal after 5 h of exposure, and then cells lost the cellular matrix and spindle shape gradually (Fig. 1C–E, respectively). Cells became spherical shape with spherical nuclei (Fig. 1F) and stopped the cell motility (Supplemental Video 1). Moreover, dead cells were suspended in the culture medium. Cells retained to rounded shape and gradually regained the cellular matrix, spindle shape, and motile or migratory activity after recovery at 38 °C (Fig. 1G and Supplemental Video 1 and 2). Unlike camel cells, porcine cells were unable to retain the orginal morphology before the heat shock and cells undewent collapse and degenrative morphology at the ending of exposure to chronic heat shock (Supplemental Video 3).

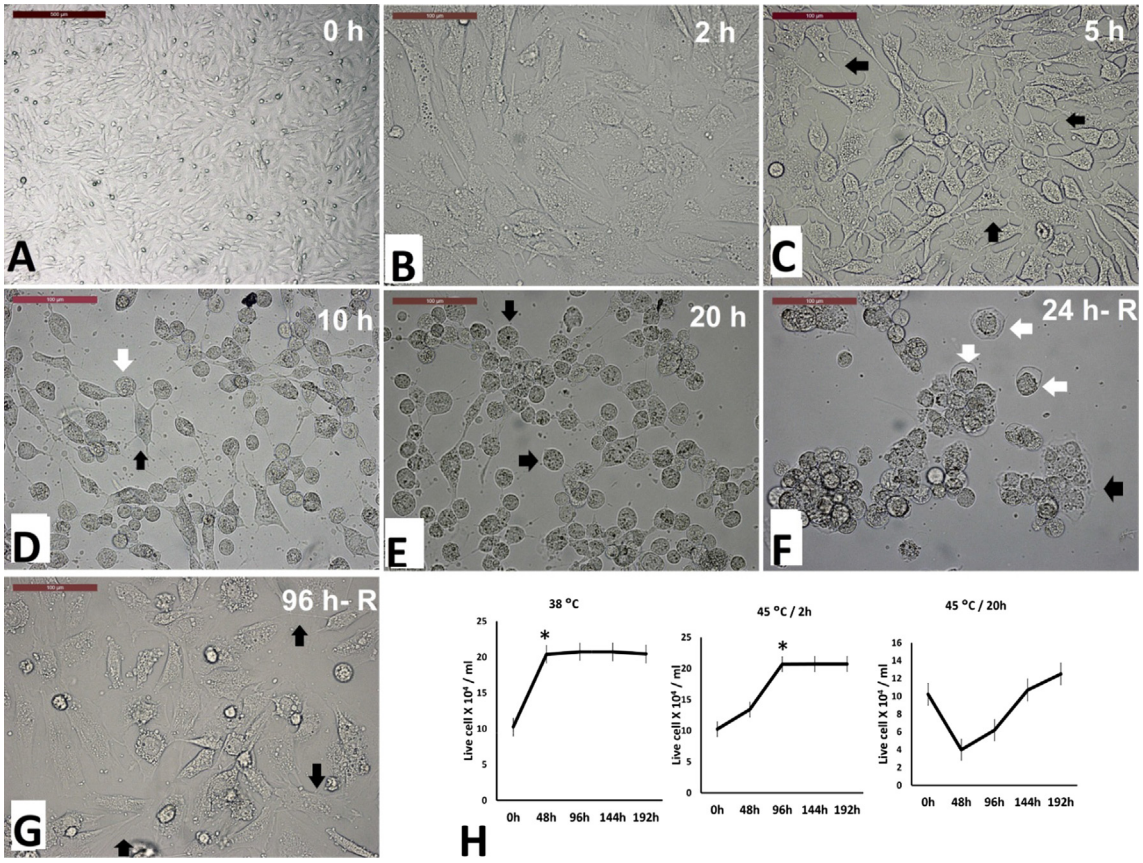

Fig. 1. Effect of acute (45 °C for 2 h) and chronic heat exposure (45 °C for 20 h) on cell morphology and proliferation. Microscopic image of cells (A) at 0 h of exposure showing spindle morphology (scale bar = 500 μm). Images B, C, D, and E showing cells after 2, 5, 10 and 20 h from exposure to 45 °C; B. cells showed no difference in morphology. C. cellular projections became string-like (arrows). D. cells turned to rounded (white arrow) shape with few cells having cellular projections (black arrow). E. Cells shows granules and cytoplasmic fragmentation (arrows). Images F and G showing the cells after 24 (24 h- R), and 96 h (96 h- R) after recovery at 38 °C; F. Cells and nuclei became enlarged (white arrow) and some cells regained attachment to the culture dish (black arrow). G. Most cells regained attachment (arrows) after 96 h of recovery and resume similar spindle morphology before heat shock. Scale bar = 100 μm. H. Cell proliferation after exposure to different heat treatments (A, 38 °C; B, 45 °C for 2 h; C, 45 °C for 20 h). Viable cells were counted using the trypan blue exclusion method every 2 days. Asterisk (*) indicates the confluency stage. Cells exposed to 45 °C for 20 h reached confluency after 244 h (data are not shown).

Proteomic profiling of heat shocked cells' proteins

The total number of proteins identified during acute heat shock exposure was higher than in the control sample (391 vs. 321, respectively). While, there was a significant decrease ($P \leq 0.05$) in the number of identified proteins in chronic heat shocked cells compared with control as well as recovered cells (178 vs. 613, and 327, respectively). The relative low number of proteins identified is due to the small database of Arabian camel proteins (Swissprot; 35 proteins, TrEMBL; 427). Comparison between the experimental groups showed that 137 proteins were unique to acute heat-shocked cells, while 67 proteins were unique to the control group (Fig. 2A). Similarly, 13 proteins were unique to the chronic heat-shocked cells and 48 proteins only appeared in the cells after recovery at 38 °C for 24 h (Fig. 2B). Proteomics analysis also showed slight differences between the number of associated peptides and peptide spectrum match (PSM) in both acute and chronic heat shocked cells (Fig. 2C and D, respectively). Fig. 3, shows the top 20 significantly dysregulated proteins reported in heat map in both acute and chronic heat-shocked cells. Total ion chromatography (TIC) and Information Dependent Acquisition (IDA) of cells after recovery from chronic heat shock showed prominent expression of heat shock protein 1 reported in cells recovered at 38 °C (Fig. 4). Details of the uniquely expressed proteins are discussed below. Further details on the full proteome profiles of all experimental groups can be found in Supplementary Excel Files 1 and 2. The mass spectrometry proteomics data have been deposited to the ProteomeXchange Consortium *via* the PRIDE [19] partner repository with the dataset identifier PXD012159. Detailed results of the proteomics are illustrated below within the discussion of some selected pathways.

Impact of heat shock on mRNA transcripts expression

Exposure of cells to 45 °C for 4 h showed that *HSP70* and *HSP90* transcripts increased 10-fold and 7-fold, respectively (Fig. 5). However, no significant alteration in *BAX*, *BCL2*, *P53*, and *ACTB* expression after acute heat shock exposure (Fig. 5). *TGFB, ACTA2, TAGLN,* and *TPM1* mRNA transcripts showed significant decrease in heat-shocked cells when compared with control cells (Fig. 5)

Role of actin polymerization during acute heat shock

We therefore, examined the effect of heat shock on the cytoskeleton by suppressing actin polymerization with cytochalasin B (CB) [20] during acute heat shock. Untreated cells exposed to 45 °C for 2 h showed no morphological changes. However, cells treated with CB during heat shock (45 °C) exhibited severe cellular shrinkage (Fig. 6E) compared to cells treated with CB and exposed to 38 °C (Fig. 6D). Two hours after removal of CB, cell morphology returned to the normal pre-exposure form, but the cells still exhibited cytoplasmic retractions (Fig. 6). Moreover, heat shocked cells treated with CB showed reduced cellular movement and healing of cell scratches after recovery at 38 °C for 24 h and 48 h (Fig. 7) compared to cells treated with CB and exposed to 38 °C or exposed to heat shock without CB treatment.

Role of Rho-associated protein kinases (ROCKs) in acute heat shock

Interestingly, treatment of cells with Y-27632, a specific selective inhibitor of Rho-associated protein kinases (ROCKs), exaggerated the effect of acute heat shock (45 °C for 2 h) on cultured cells. Cells showed cytoplasmic retractions and shrinkage and turned into star-shape (Fig. 8). Moreover, the ROCK inhibitor (RI)

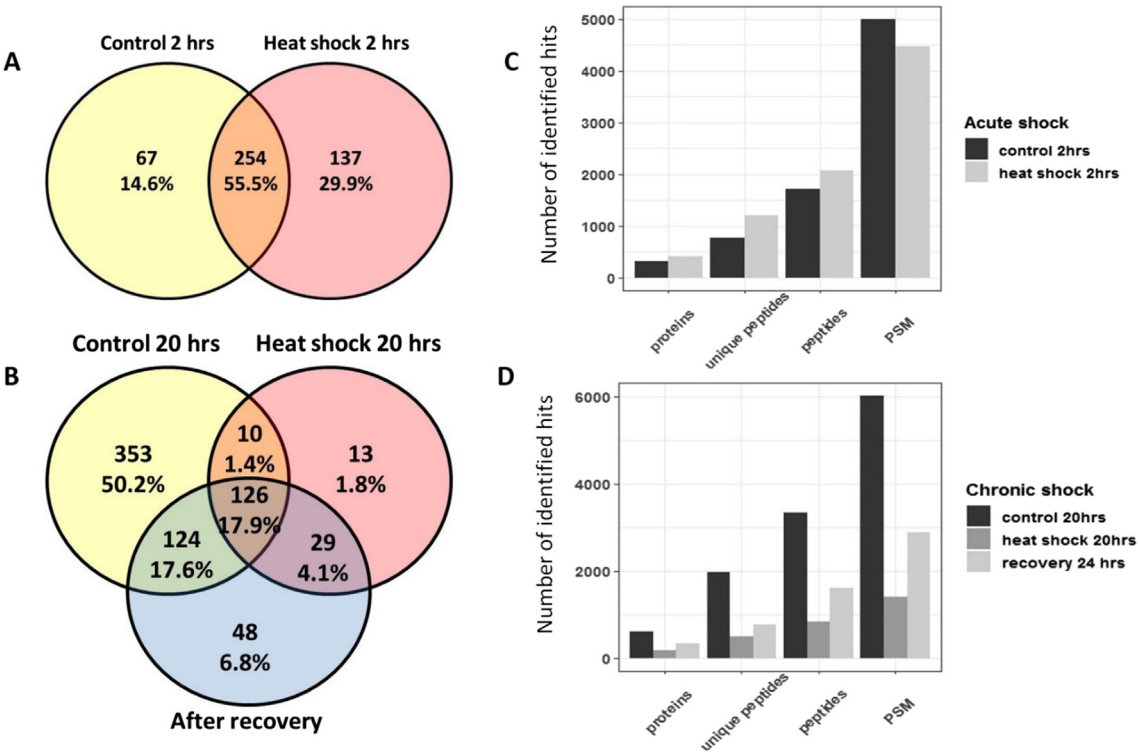

Fig. 2. Comparative proteomic profiling of camel cells exposed to acute and chronic heat stress. (A and B) are Venn diagrams of the acute and chronic experiments, respectively, showing the numbers and percentage of non-redundant proteins. (C and D) are bar plots of identified proteins, unique peptides, total peptides and corresponding Ms/Ms spectra in both acute and chronic experiments, respectively.

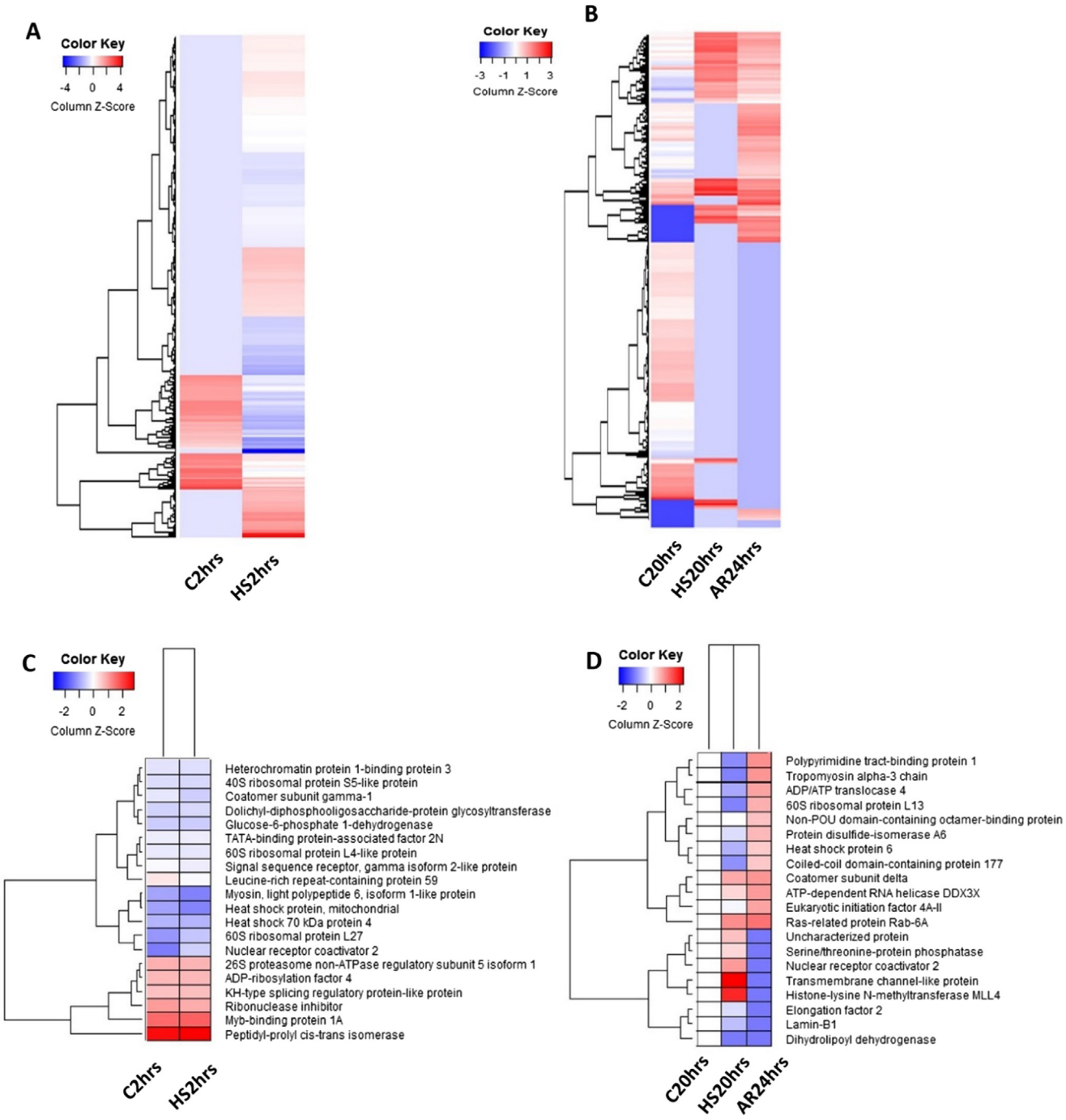

Fig. 3. Heat-map analysis showing protein normalized spectral abundance factor (NSAF) for identified proteins of camel cells subjected to acute heat stress (A) or chronic heat stress (B). Abundances of the top 20 dysregulated proteins for both acute and chronic exposure are illustrated in panels (C and D), respectively. Data are normalized, log transformed and scaled. C2hrs: control group at 38 °C for 2 h 2 h, HS2hrs: heat shock for at 45 °C for 2 h, C20hrs: control group at 38 °C for 2 h after 2 h, HS20hrs: heat shock at 45 °C for 2 h, and AR24hrs: after recovery at 38 °C for 24 h.

Y-27632 retarded wound healing of cells exposed to the acute heat shock (Fig. 9) more than CB treatment (Fig. 7); wound width was 525.23 ± 34.2 vs. 790.16 ± 24.3 in CB and RI, respectively.

Role of transforming growth factor pathway in chronic heat stress

We hypothesized that the TGFβ pathway, which is related to cytoskeleton organization, might be involved in the morphological changes associated with the cellular response to chronic heat shock. Interestingly, supplementation of the culture medium with SB-431542 (a TGFβ pathway inhibitor) maintained the spindle morphology of the heat-tolerant cells (Fig. 10) when compared with non-supplemented cells. Cells resumed replication after 120 h of recovery as illustrated in Fig. 1D–G.

Impact of heat shock on oxidative stress, anti-oxidative defense, apoptosis and cell viability

Acute exposure of cells to 45 °C for 2 h showed no effect on malondialdehyde (MDA) levels; however, chronic exposure to 45 °C for 20 h increased MDA over its level after 2 h of exposure (3.88 nM/mL vs. 3.02 nM/mL, respectively, $P \leq 0.05$). In contrast,

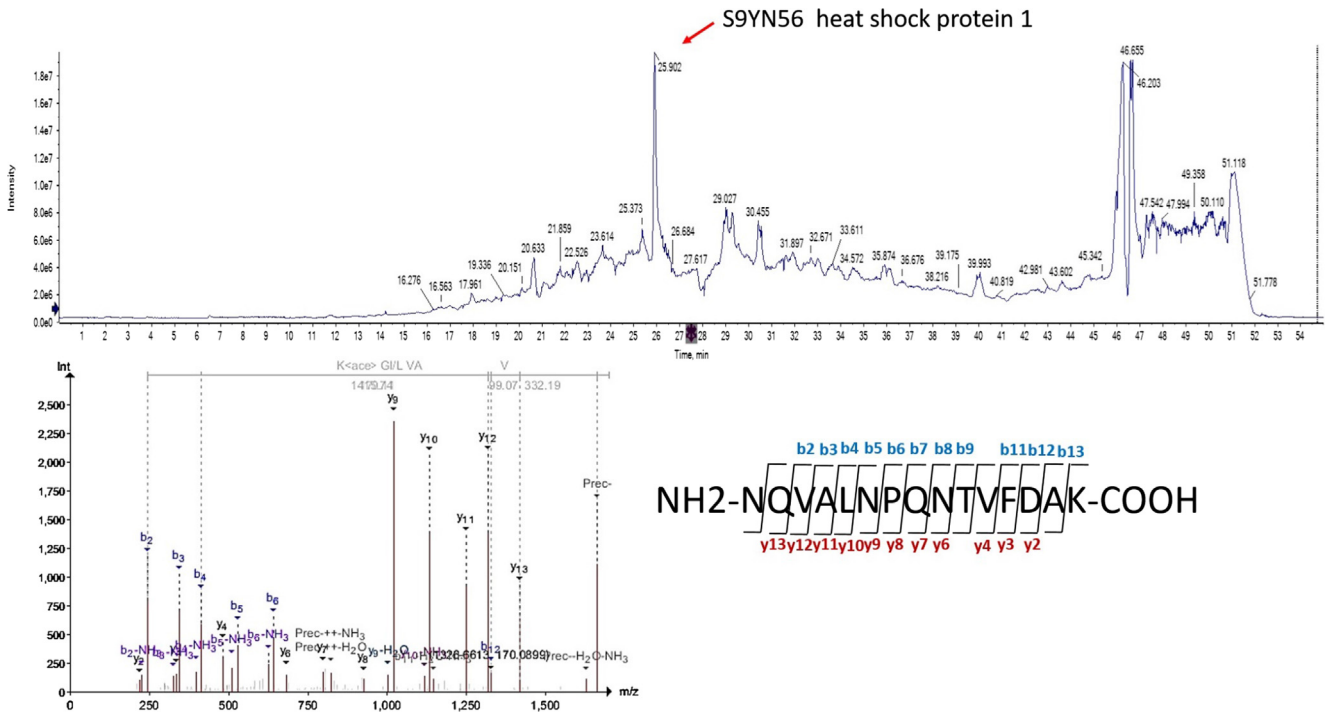

Fig. 4. Total ion chromatography (TIC) and Information Dependent Acquisition (IDA) of cells after recovery from chronic heat shock. TIC [upper panel] and representative annotation of tandem mass spectrometry (MS/MS) spectra [lower panel] of the $[M + 2H]^2$ ion for the peptide NQVALNPQNTVFDAK of heat shock protein 1 reported in 'after recovery' group.

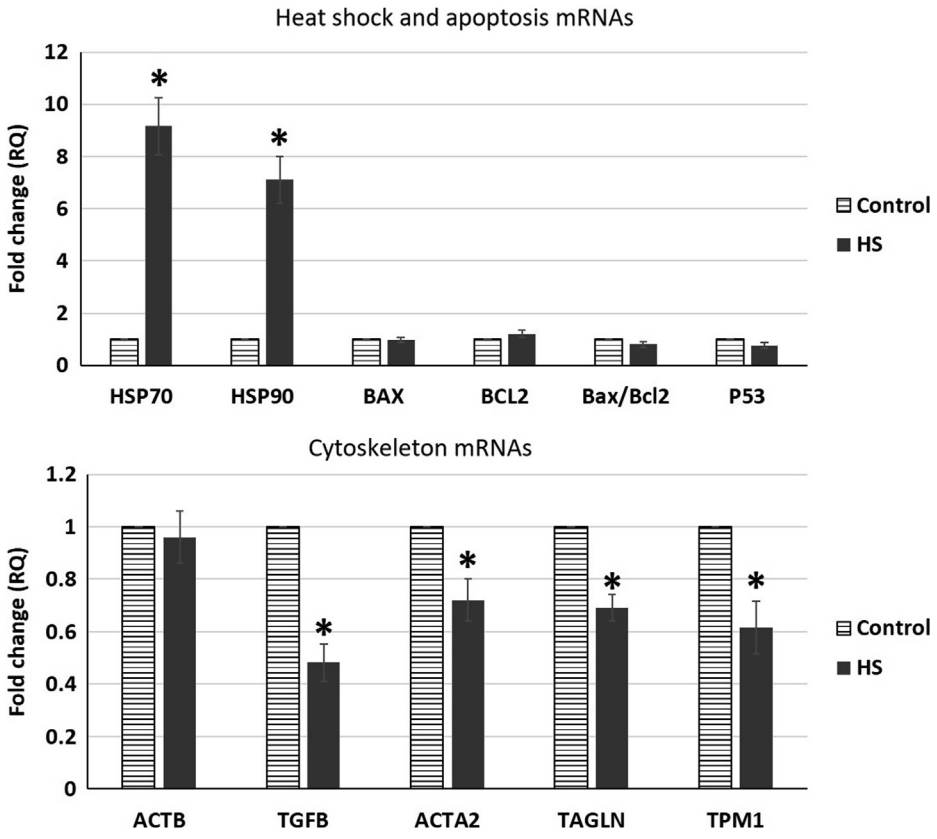

Fig. 5. The effect of heat shock (45 °C for 4 h) on the expression of mRNA transcripts. The relative quantification (RQ) of *HSP70*, *HSP90*, *P53*, *BAX*, *BCL2*, *ACTB*, *TGFB*, *ACTA2*, *TAGLN*, and *TPM1* mRNA transcript was normalized to the *GAPDH* level in the control cells (cultured at 38 °C). Superscripts (a and b) indicate significant differences ($P \leq 0.05$) between transcript in each column.

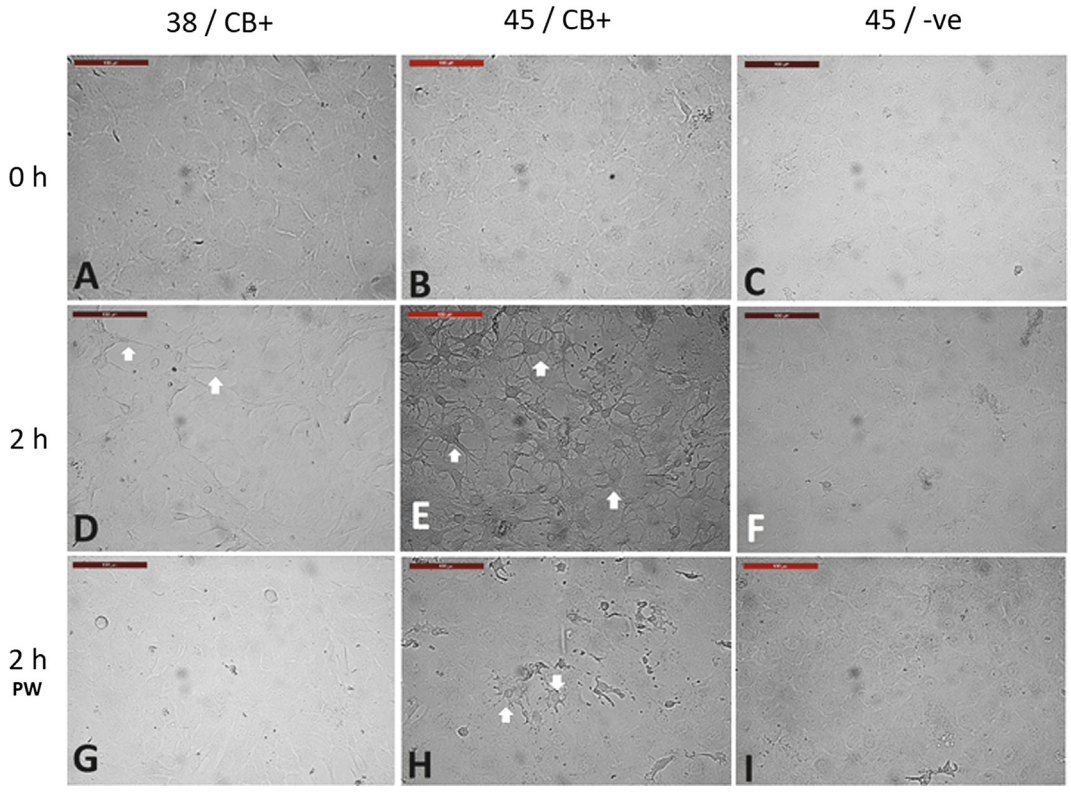

Fig. 6. Effect of cytochalasin B on acute heat shock of camel cells. (A) cells were incubated at 38 °C and with 0.5 mg/mL cytochalasin B (CB). (B and C) Cell were treated with or without CB at 45 , respectively. (D, E, and F) Images of A, B, and C, at the end of heat treatment for two hours. CB at 38 °C caused cell shrinkage (D. arrows), the effect was exaggerated at 45 °C (E. arrows). (F) shows no morphological changes of cells exposed to 45 °C without addition of CB. (G, H, and I) show the cells two hours post-washing (PW) and medium replacement without CB in all treatments. Cells were microscopically examined for identifying the effects of CB. (H) Cells exposed to 45 °C in the presence of CB show cell degeneration and disturbed architecture (arrows). Scale bar = 100 μm.

GSH levels increased significantly after acute exposure to 45 °C for 2 h (145.2 mM/L vs. 126.4 mM/L, $P \leq 0.05$) with no difference at the end of chronic exposure for 20 h (Table 1).

Discussion

The current study revealed the molecular mechanism of the camel cells to manage and recover from acute and chronic heat shock and showed the adaptability of camel somatic cells to conserve life under extremely hot conditions. The disturbed architecture of camel cells exposed to extremely chronic heat shock (45 °C for 20 h) might be indicative of a special cellular restructural response by camel cells. Similar morphological changes were reported in rat intestinal cells exposed to 42 °C for 4 h [9] and amoeba cells exposed to acute heat shock at 34 °C for 30 min [21]. Notably, after recovery at 38 °C, the morphological changes were gradually disappeared, and the camel cells returned to their normal spindle morphology and migratory activity, which indicates a unique feature of camel cells resilience and plasticity that has not been reported for other mammalian cells.

Proteomics results showed that the level of nuclear receptor coactivator 2 increased 2-fold ($P \leq 0.05$) in acute heat shocked cells. Nuclear receptor coactivator 2 is involved in protein dimerization, intracellular receptor signaling, and regulation of DNA transcription as a cellular defense against the protein denaturation associated with heat shock [22]. A significant decrease in leucine-rich repeat-containing protein 59 was observed in acute heat shocked cells. This might be associated with reduced RNA trafficking and binding to the ribosomes and a pause of ribosome translation that occurs with heat shock [23,24]. Interestingly, chronic heat shock altered several proteins in the experimental groups (Fig. 3B and D). Coatomer subunit delta, Ras-related protein Rab-6A helicase and ATP-dependent RNA helicase DDX3X were all significantly elevated by chronic heat shock and were not detected in control cells. These proteins are responsible for intracellular protein transport, retrograde vesicle-mediated transport Golgi to ER, and ATP-dependent RNA helicase activity, a response reflecting the protein turnover stimulated by heat shock. Moreover, the heat shock and recovery stages induced eukaryotic initiation factor 4A-II which is involved in the cellular response to osmotic stress and stress granule assembly. These four proteins maintained their elevated expression after recovery from chronic heat shock. Similarly, chronic heat shock induced proteins such as nuclear receptor coactivator 2 previously discussed in the acute heat shock. In addition, it uniquely induced expression of transmembrane channel-like protein and histone-lysine N-methyltransferase MLL4 which regulate calcium ion transmembrane transport and transcription. The levels of these three proteins steeply decreased during the recovery stage and so may be induced by chronic heat shock (Supplementary Excel File 2).

During acute heat shock, results of qPCR showed no significant alteration in *ACTB* expression (Fig. 5) and similarly proteomics results showed non-significant decrease in the level of beta-actin (0.5-fold) after exposure to acute heat shock (Supplementary Table 2). This result might indicate a high turnover of the beta actin protein during heat shock or suggests the existence of another supportive pathway to maintain the cytoskeleton integrity (Fig. 1B). Two hours after removal of CB, cell morphology returned to the normal pre-exposure form [25], but the cells still exhibited cyto-

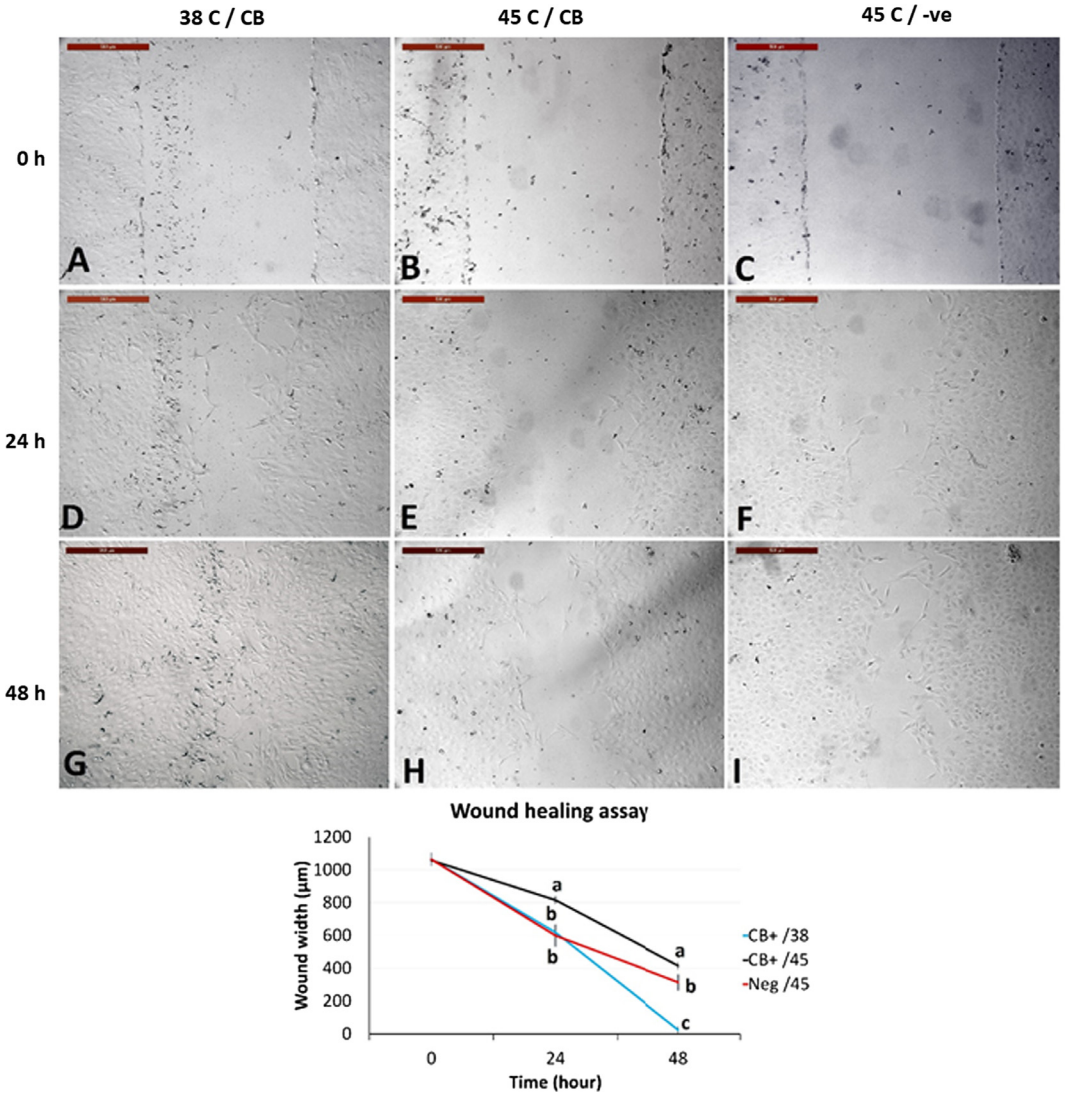

Fig. 7. The effect of supplementing with cytochalasin B during acute heat shock on wound healing assay. (A–C) represent cell monolayers at 0 h after wound healing. (D-F) Cells after 24 h of culture at 38 °C. (G–I) Cells after 48 h of culture at 38 °C. (A, D, and G) CB-treated cells for 2 h at 38 °C. (B, E, and H) CB-treated cells for 2 h at 45 °C. (C, F and I) Non-treated cells cultured for 2 h at 45 °C. (J) Results of wound healing and wound closure in the three treatments in μm, lines at specific duration (24 and 48 h) carrying different letters (a, b, and c) are considered statistically different ($P < 0.05$). Scale bar = 500 μm.

plasmic retractions which indicate that cytoskeleton integrity during heat shock, particularly dynamic actin polymerization, is involved in the cellular defense against acute heat shock.

Furthermore, the current results indicate additional essential roles of the ROCKs pathway not only in maintaining actin polymerization and the cell cytoskeleton but also for actomyosin activity [26,27] as a mean of defense against acute heat shock. This finding coincides with the results reported by Ramachandran et al. (2011) who found that RI treatment resulted in the loss of stress fibers and caused cellular shrinkage and stellate appearance of the cells [28]. Digging the Rho signaling pathway through proteomics (Supplementary Table 4) revealed that spetins (spetin 2, 7 and 9) disappeared after acute heat shock. Septins connect to Cdc42 effectors, Borg proteins, and are involved in cytokinesis and cell division, which could explain the delay in wound healing by RI-treated acute heat shocked cells [29]. On the other hand, there was no change in cofilin-1 after acute heat shock, suggesting the maintenance of actin polymerization [30] during the response against heat shock. Conversely, most Rho-associated proteins (such as septins, F-actin, myosin heavy chain, transforming protein RhoA, and Rho GDP-dissociation inhibitor 1) were absent; in addition, the extreme reduction (3-fold) of cofilin-1 after chronic heat shock (Supplementary Table 5) indicated the loss of stress fibers and actomyosin integrity and may account for the observed morphology of cells after chronic heat shock (Fig. 1D–F). Cytoskeletal actin and stress fibers are not static and can easily change cell morphology by assembling or disassembling themselves [31]. Moreover, tubulin polymerization is susceptible to temperature change; early experiments revealed that most microtubules in animal cells disassemble when the cells are cooled to 4 °C and reassemble when the cells are rewarmed to 37 °C, and these changes are regulated by microtubule-associated proteins (MAPs) [31].

Although, qPCR results demonstrated that acute heat shock caused no alteration in *ACTB* expression, it significantly decreased ($p \leq 0.05$) the expression of *TGFB*, *ACTA2*, *TGLN*, and *TPM1* (Fig. 5). Although we noticed a reduction in the expression of TGFβ and its pathway (actinin 2, transgelin, and tropomyosin) transcripts, the acute effects of elevated temperature were not clearly reflected on the proteomics level (Supplementary Table 2). Most probably, effects on the protein level might require more time as evidenced in the chronic heat shock results (Supplementary Table 3). Meanwhile, Flanders et al. showed that hyperthermia

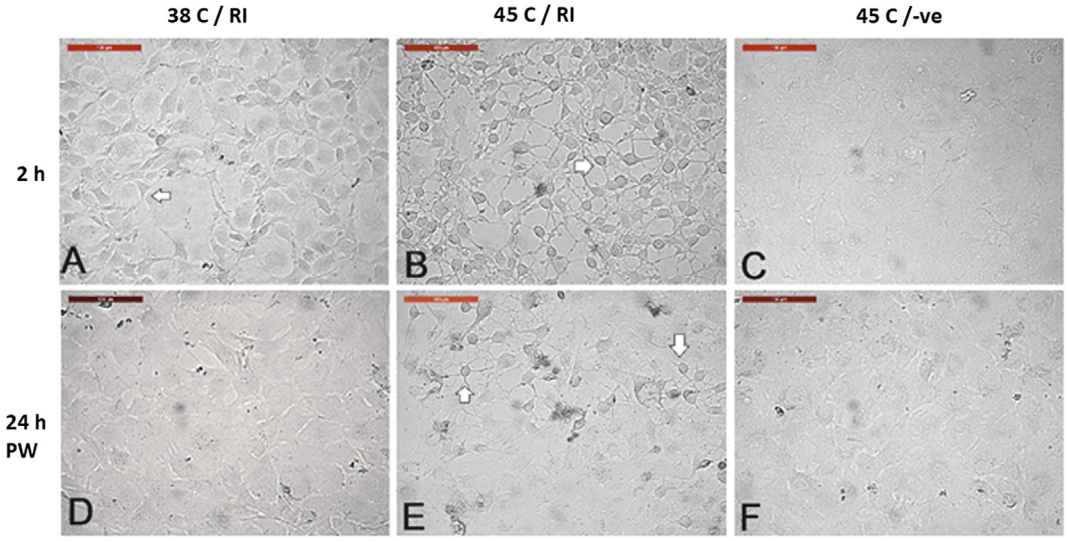

Fig. 8. Effect of ROCK-inhibitor (RI) on acute heat shock of camel cells. (A) Cells were incubated at 38 °C and treated with RI for two hours. (B, C) Cells were incubated at 45 °C treated with or without RI, respectively. RI at 38 °C caused cell shrinkage (A. arrow), the effect was exaggerated at 45 °C (B. arrow). (D, E, and F) Images of A, B, and C 24 h post-washing (PW) and medium replacement without RI and recovery at 38 °C. Cells showed star-shape and shrinkage in RI-treated heat shocked cells (arrows). Scale bar = 100 μm.

(41.5 °C for 2 h) was associated with TGFβ induction at the mRNA and protein levels in cardiac rat cells as a cardioprotective effect of heat shock [32]. In the current study, supplementation of the culture medium with SB-431542 maintained the spindle morphology of heat-exposed cells with no effect on cell replication after 120 h of recovery. *TAGLN*, *ACTA2*, and *TPM1* are TGFβ-inducible genes and are required for actin cytoskeleton organization and cellular differentiation [33], but their involvement in cellular morphological acclimation to heat stress is not known. SB-431542 specifically inhibits the activin receptor-like kinase activity of ALK-4, ALK-5, and ALK-7 [34]. Studies have shown that supplementation with a TGF-β antagonist (recombinant TβRII/Fc chimera) ameliorated the heat-induced blood-testis-barrier disruption, which reflected the involvement of *TGFB* expression in heat-induced morphological changes in the testis [35]. We propose that the TGFβ pathway might be involved in the disruption of cellular architecture and this impact can be alleviated through inhibition of the TGFβ pathway. Our results coincide with those of Wang et al. [36], who found around 2- to 4-fold reduction in transgelin (*TAGLN*) expression in chicken testis after acute heat shock, while they contradict the results of He et al. [37] who found a 1.6-fold increase in rat intestinal *TAGLN* expression after acute heat shock (41 °C for 2 h). These two results are conflicting probably because the internal core body temperature of chicken and rats differs and both are different from the in vitro conditions in this study. Additionally, several proteins involved in the TGFβ pathway and expressed during heat shock maintained altered expression levels after recovery (Supplementary Table 6); A-kinase anchor protein 12, mastermind-like protein, actinin 2, transgelin, and serpin showed ~ 0.5-fold decrease after chronic heat shock, while tropomyosin 1 showed no alteration after chronic heat shock. Interestingly, these changes were partially restored during the recovery stage particularly serpin and mastermind-like protein levels which increased by 2-fold and 1.5-fold respectively, when compared to their levels after heat shock (Supplementary Table 7).

Chronic heat shock diminished proteins associated with cytoskeletal integrity such as integrin alpha V, fermitin, moesin, clathrin, dynein, and plastin-2, all of which are involved in cell adhesion and cytoskeletal organization and they reappeared after cell recovery at 38 °C. Additionally, the protein talin, which is associated with actin binding, disappeared after chronic heat shock and did not return during the recovery stage. Importantly, galectin levels markedly decreased after chronic heat shock and recovery by 4- and 7-fold, respectively, (Supplementary Table 3) when compared with expression in control cells, suggesting the loss of integrin binding and subsequently low cellular adhesion [38].

Moreover, proteomics results showed that during acute heat shock expressed cell adhesion protein integrin alpha V (Supplementary Table 2), paradoxically however chronic heat shock inhibited integrin alpha V (Supplementary Table 3). In contrast, during the recovery stage there was a decrease (0.25-fold) in elongation factor 2 (Fig. 3), which aids in actin filament binding, cadherin binding, and is involved in the response to endoplasmic reticulum stress. In addition, lamin-B1, which is a component of the nuclear lamina and provides a framework for the nuclear envelope and may also interact with chromatin, also decreased (0.5-fold) during recovery. Interestingly, beta-actin expression increased 1.7-fold during the recovery stage compared with heat shocked cells (Supplementary Table 3). Some proteins disappeared during chronic heat shock and resumed their expression during the recovery stage including integrin alpha V, moesin, clathrin, dynein, and plastin-2 which are involved in cell adhesion and cytoskeletal organization. Additionally, the protein talin, which is associated with actin binding disappeared after chronic heat shock and was not regained during recovery. Some proteins were induced by heat shock and maintained their expression during the recovery stage including heat shock protein 6, which is involved in protein folding and alpha-crystallin, which had a 3.2-fold increase during the recovery stage and is responsible for nuclear and cytoplasm structure (Supplementary Table 3).

It is well known that heat shock is considered as an oxidative stress. Shotgun proteomic profiling pinpointed a significant increase in glutathione S-transferase mu and P1-1 (1.6- and 3.3-fold, respectively) (Supplementary Table 2) after acute heat shock. Additionally, after recovery from chronic heat shock, cells resumed their expression of both enzymes (Supplementary Table 3), as a cellular defense to the increased level of MDA caused by chronic heat shock (Table 1). This response is essential to prevent intracellular damage caused by reactive oxygen species and as a powerful defense against lipid peroxidation and the breakdown of xenobiotics [39,40]. Exposure to heat for 2 h inhibited cell proliferation for 24 h, then cells gained their ability to proliferate and reached

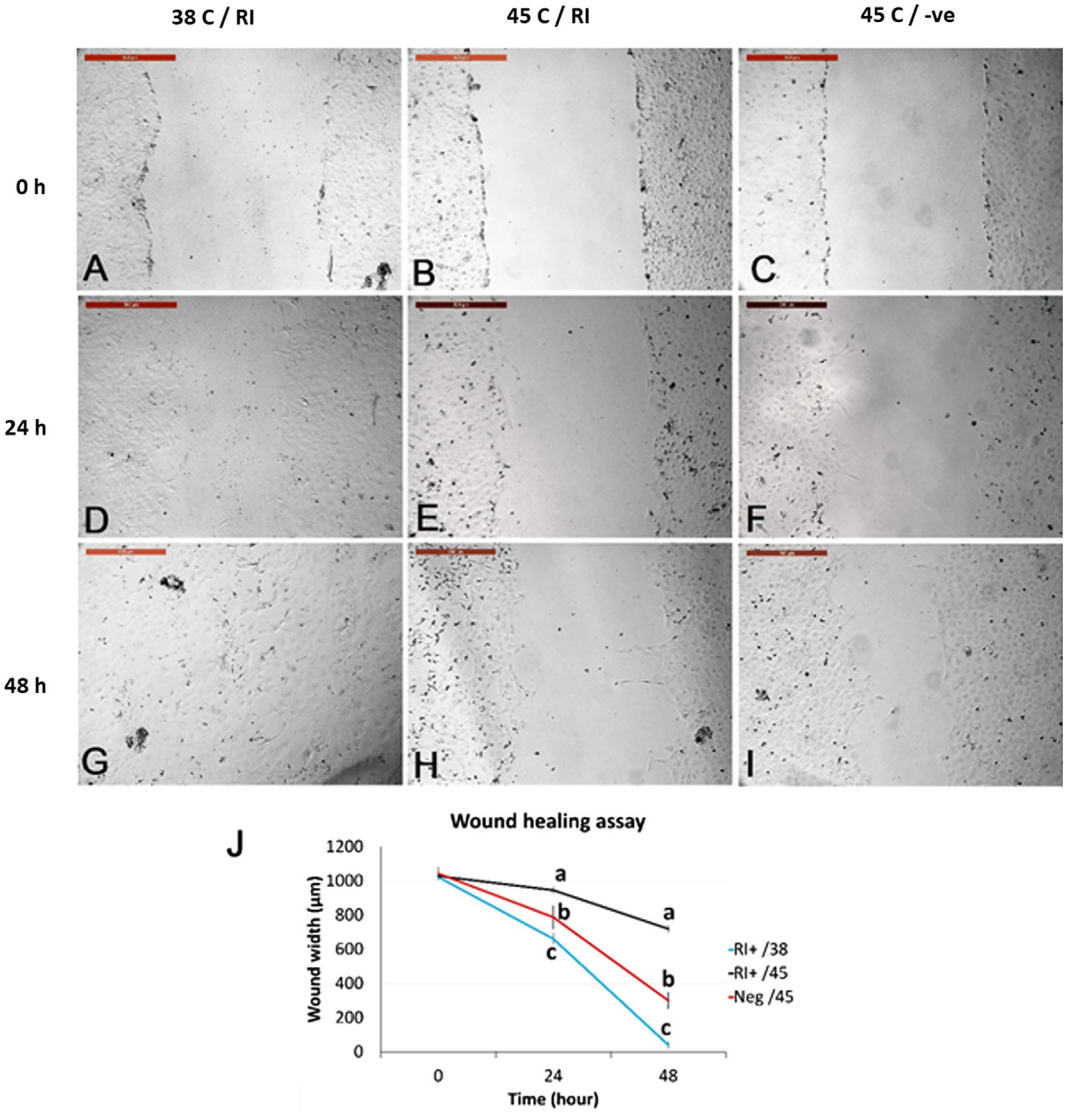

Fig. 9. The effect of supplementing ROCK-inhibitor Y-27632 (RI) during acute heat shock on wound healing assay. (A–C) Cell monolayers 0 h after wound healing. (D–F) Cells after 24 h at 38 °C. (G–I) Cells after 48 h at 38 °C. (A, D, and G) RI-treated cells for 2 h at 38 °C. (B, E, and H) RI-treated cells for 2 h at 45 °C. (C, F, and I) non-treated cells cultured for 2 h at 45 °C. (J) results of wound healing and wound closure in cells of the three treatments in µm. Scale bar = 500 µm. Lower case letters (a, b, and c) indicate significant differences at $P < 0.05$.

confluence at 96 h post heat stress. Afterwards, the cells behaved in a similar matter to those in the control group (Fig. 1H). This result confirms the finding of Figs. 7 and 9 because heat shocked cells (non-treated with CB or RI) showed reduced the wound healing capability compared with those cultured at 38 °C. Conversely, prolonged heat stress decreased the viability (living cells were reduced to 32% compared to 100% pre-exposure) and proliferation of cells for 48 h post heat stress (Fig. 1C). These cells resumed replication 144 h post heat stress but did not reach confluence until 240 h post-exposure (data not shown). As we show below, and in accordance with the MIQE guidelines [41], chronic heat shock significantly decreased Gapdh and actin-β proteins and therefore we did not perform real-time PCR analysis for the chronic heat shocked cells and only showed the results of the proteomics profile. Further investigations are required to determine which housekeeping genes are not altered by chronic heat shock and can be used as reference controls for relative quantification of mRNA transcripts.

Interestingly, *P53*, *BAX* and *BCL2* transcripts as well as the *BAX*/*BCL2* ratio showed no change after acute heat shock (Fig. 5). Among the unique proteins that were found as a response to the acute heat shock (Supplementary Table 2), were some associated with apoptosis and autophagy such as 26S protease regulatory subunit 6A, 26S proteasome non-ATPase regulatory subunit 5 isoform 1, cathepsin D, cullin-associated NEDD8-dissociated protein 1, cytochrome *c*, nucleosome assembly protein 1-like 1 isoform 2, poly [ADP-ribose] polymerase, proliferation-associated protein 2G4, proteasome subunit beta, and Ras-related protein Rab-2A, suggesting a cellular response to the short-term exposure to heat shock through apoptosis and autophagy (Supplementary Excel File 1). We propose that cells respond to acute heat shock by brief arrest in cell cycle to permit the corrections of cellular damage caused by the heat shock. Additionally, prohibitin-2 increased 1.5-fold during chronic heat shock and 2-fold during the recovery stage (Supplementary Excel File 2), indicating the mitophagy stimulation was a response to the heat shock injury [42].

Moreover, acute heat shocked cells also expressed unique proteins associated with protein folding such as DNA damage-binding protein 1, heat shock 70 kDa protein 4, heat shock protein 70 A1B, and heat shock protein 90, as well as proteins involved in ubiquitination such as ubiquitin thioesterase and ubiquitin-conjugating enzyme E2 variant 2 (Fig. 3 and Supplementary Excel

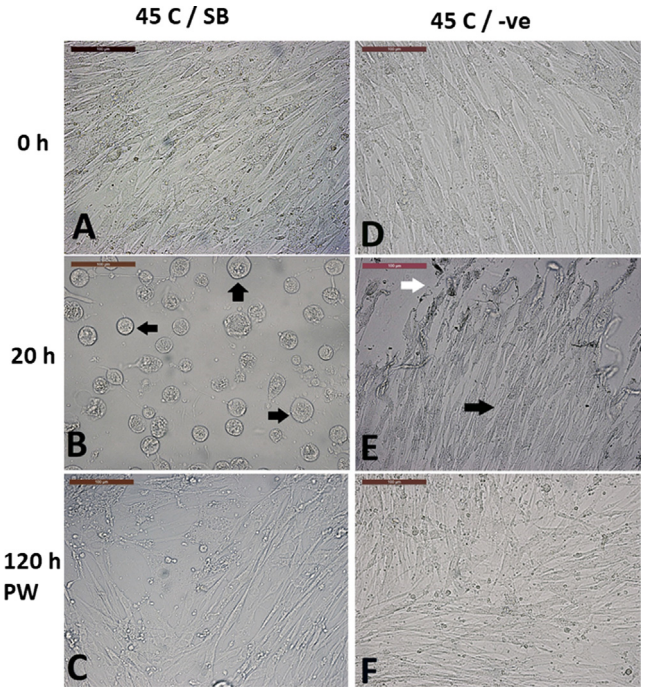

Fig. 10. Effect of SB-431542 (TGFβ inhibitor) on cell morphology and replication after exposure to chronic heat shock. (A–C) cells cultured without SB-431542 (SB) supplementation, while (D–F) show cells cultured with SB-431542. (A and D) show cells before heat treatment. (B and E) show the cells after exposure to 45 °C for 20 h. (B) Cells have a rounded enlarged morphology with enlarged nuclei (black arrows), while in (E) cells maintained their spindle morphology (black arrow) degenerated cells were present (white arrow). (C and F) cells regained spindle morphology and replication 120 h post-washing (PW) and medium replacement without SB-431542 and recovery at 38 °C. Scale bar = 100 μm.

File 1). Heat shock proteins are chaperones cause partial unfolding or protein aggregation that protect cells from the detrimental thermal and oxidative stress [43]. Hsp70 and other HSPs bind to hydrophobic residues exposed by stress and prevent partially denatured proteins from aggregation and allow them to refold [44]. Furthermore, HSPs stabilize and protect actin microfilaments when organized in small, phosphorylated oligomers [3]. Chronic heat shock significantly ($P \leq 0.05$) increased chaperons levels including endoplasmin (Hsp90b1), heat shock protein 70 A1B, heat shock protein 90, and heat shock protein beta-1 compared to control cells by 1.35-, 1.45-, 1.54-, and 1.7-fold respectively. Heat shock protein 70 1A and heat shock protein 70 1L increased during the recovery stage compared with their levels in heat shocked cells (1.4-fold of both) (Fig. 2 and Supplementary Excel File 2). Interestingly Hsp70 (heat shock protein 1) elevated dramatically in the recovery stage. Fig. 4 shows an obvious peak of Hsp70 through TIC and IDA analysis that indicates the essential roles of chaperones during the stage of recovery for protein refolding and corrections of misfolding that were associated with the chronic heat shock. We propose that maintaining high levels of Hsp70 during the exposure to such high temperature is the major cell machinery required for protection of cellular proteins from the damaging thermal stress. In addition, upregulation of Hsp70 during recovery may also suppress DNAase activity associated with chronic heat shock [12,45] and may also share in the cell cycle arrest [45] that was found in our results to allow the DNA repair. Conversely, PCR results showed that acute heat shock did not affect the expression of *P53*, *BAX*, and *BCL2* (Fig. 4). Apoptosis can be inhibited with Hsp70 *via* blocking the binding of procaspase-9 to the cytochrome *c* apoptosome complex [46]. Moreover, Hsp70 augments the glutathione reductase activity to reduce glutathione disulfide into sulfhydryl form of glutathione (GSH). This interplay augments the cytoprotective effects of Hsp70 and the cellular redox environment in response to stress [47]. Camel somatic cells mitigate the impacts of acute heat shock by increasing the expression of heat shock proteins and GSH levels. This observation is in accordance with earlier genomic studies which illustarated the adaptation of camel genome to extreme environmental heat [6]. Additionally, chronic heat shock induced the expression of other chaperons such as *HSP6* (Supplementary Table 3), serine/threonine-protein phosphatase, and nuclear receptor co-activator-2 (Fig. 3D), which were maintained during the recovery stage. Moreover, during the recovery stage chaperon proteins associated with protein folding such as protein disulfide-isomerase A6 increased (1.5-fold) when compared to the heat shock stage (Fig. 3).

Heat shock and recovery also selectively evoked some proteins associated with metabolic pathways such as ADP/ATP translocase 4, which exchanges cytosolic ADP for mitochondrial synthesized ATP. It uniquely induced dihydrolipoyl dehydrogenase which is involved in fatty acid oxidation, lipoprotein catabolism and proteolysis [48]. Additionally, chronic heat shock uniquely induced proteins associated with nucleic acid metabolism and protein translation such as polypyrimidine tract-binding protein 1 and non-POU domain-containing octamer-binding protein. Moreover, 60S ribosomal protein L13 increased during recovery by 2.2-fold compared with the levels during heat shock (Supplementary Excel File 2). Our finding clearly show that acute heat shock uniquely induced some metabolic proteins associated with ATP synthesis such as ATP synthase protein 8 and cytochrome *c* oxidase subunit 3. Moreover, acute heat shock increased levels of DNA-(apurinic or apyrimidinic site) lyase (1.5-fold), a DNA repair enzyme. Similarly, gene ontology studies showed altered protein pathways in chronic heat shock and after recovery. For example, we reported that DNA-(apurinic or apyrimidinic site) lyase which was expressed in heat shocked cells could not detected by mass spectrometry during the recovery stage. However, some metabolic proteins resumed their expression after recovery such as ATP synthase protein 8 and Na/K ATPase (Supplementary Excel Files 1 and 2).

The morphological changes observed in the camel granulosa cell exposed to 45 °C for 20 h in this study (Figs. 1 and 10) were interesting and raise the possibility of cellular acclimation towards heat shock through an estivation-like state in the mammalian cells. Estivation is a process of thermotolerance, where many invertebrates enter a state of aerobic dormancy in response to extremely elevated environmental temperatures. This status characterized by hypometabolism associated with behavioral, physiological, and biochemical slackening. Such adaptation aim to conserve water, energy reserves, and to minimize detrimental effects to cellular machinery [49]. To confirm this hypothesis, further metabolomics studies are ongoing. Interestingly, our current results revealed that

Table 1
Levels of malondialdehyde (MDA) and reduced glutathione (GSH) in the response to acute and chronic heat shock.

	38 °C –2 h	45 °C –2 h	38 °C –20 h	45 °C –20 h
MDA (nM/ml)	3.14 ± 0.21^{b}	3.02 ± 0.1^{b}	3.19 ± 0.34^{b}	3.88 ± 0.22^{a}
GSH (mM/L)	126.4 ± 4.4^{b}	145.2 ± 4.1^{a}	123.8 ± 3.2^{b}	135.4 ± 2.1^{ab}

a, b different superscripts indicate significant differences between treatments at $P \leq 0.05$.

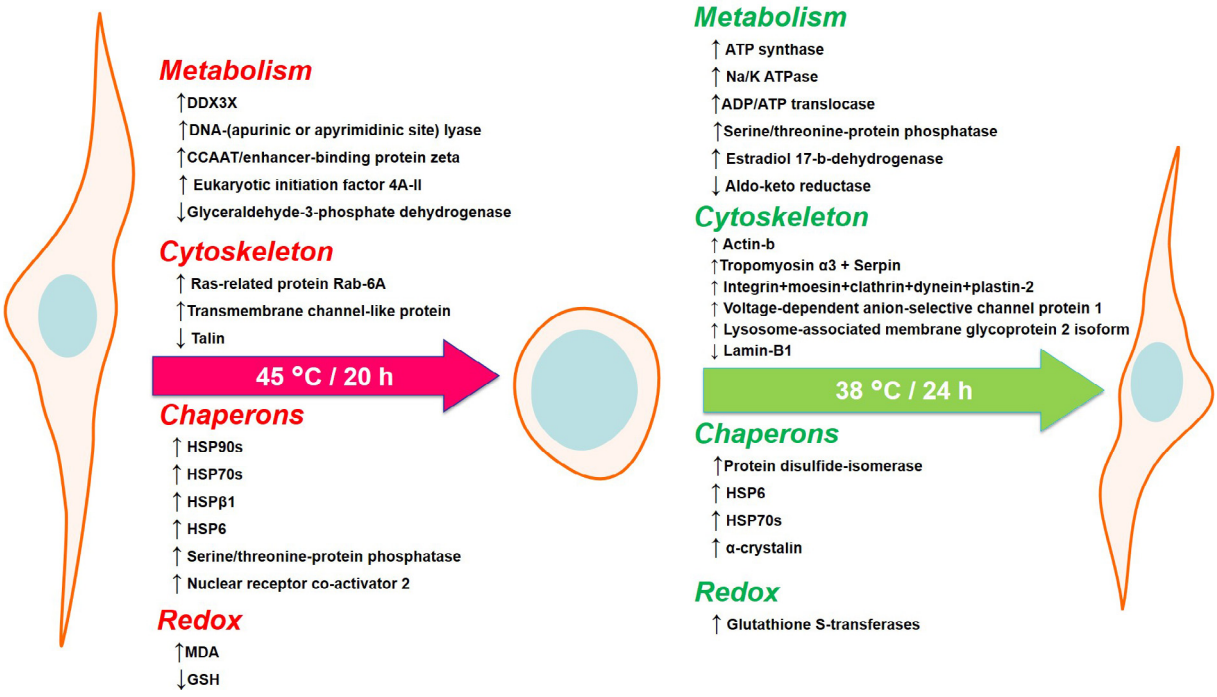

Fig. 11. Summary of major changes observed to the cells after chronic heat shock and recovery.

several metabolic enzymes were dysregulated after chronic heat shock, such as glyceraldehyde-3-phosphate dehydrogenase which is a main house-keeping gene in normal non-stressed cells [50]. Additionally, several metabolic proteins were not detected during chronic heat shock and were significantly elevated during the recovery stage such as ATP synthase and Na/K ATPase (Supplementary Table 3, Fig. 11). This might indicate that a hypo-metabolic state occurred in the cells during chronic heat exposure to a temperature considered lethal to many other mammalian cells as part of an estivation-like state that we propose in the current model. The absence of Na/K ATPase may also affect cell volume (as observed in Figs. 1 and 10) and increase the total amount of water contained in the cells during heat shock exposure [51]. The increased level of dihydrolipoyl dehydrogenase seen during chronic heat shock (Fig. 3D) indicates the dependence of the cells on the energy liberated from lipid and protein catabolism, which is associated with the current model for protection against lethal hyperthermia. Interestingly, estradiol 17-beta-dehydrogenase 1, an enzyme required for estradiol metabolism in the granulosa cells, was among the proteins that were absent in chronically heat shocked cells (Supplementary Table 3, Supplementary Excel File 2), and were restored after recovery, confirming the metabolic dormancy state of chronically heat shocked cells. The link between the "estivation-like state" that we propose here and the newly introduced phenomenon of cellular recovery "anastasis" or the cellular resurrection and reversal of cell death is interesting and requires further investigation.

Conclusions

We provide a molecular interpretation for the thermotolerance of camel granulosa cells. The common features of the cellular response to acute heat shock (45 °C for 2 h) are increasing the expression of heat shock proteins and DNA repair enzymes. Whereas cells exposed to chronic heat shock (45 °C for 20 h) showed reduction in total protein levels, metabolic enzymes, and cytoskeletal proteins. These alterations were partially restored during the recovery stage after 24 h with an obvious increase in Hsp70 and then cells regained their normal cellular morphology on the 9th day of recovery (Fig. 11). The strategy of cellular defense and tolerance to both thermal conditions reflects the flexible adaptability of camel cells. The cellular resilience, plasticity and mechanism of recovery from chronic heat stress can be an example for understanding the interesting newly discussed phenomenon "anastasis" [52]. This strategy would also provide a paradigm for interfering with the thermotolerant response of cells that may occur in certain diseases such as tumors [53].

Funding

This study was supported by King Saud University, Deanship of Scientific Research, Research Group #RG-1438-018. The work was partially funded by ECN-USA to SM.

Declaration of Competing Interest

Author declares that there is no conflicts of interest.

Acknowledgments

The authors thank Prof. Goo Jang, College of Veterinary Medicine at Seoul National University, South Korea, for facilitating the time-lapse cell imaging. The authors extend their appreciation to the RSSU, Deanship of Scientific Research at King Saud University, Saudi Arabia, for technical assistance.

Appendix A. Supplementary material

Supplementary data to this article can be found online at https://doi.org/10.1016/j.jare.2019.11.009.

References

[1] Samali A, Holmberg CI, Sistonen L, Orrenius S. Thermotolerance and cell death are distinct cellular responses to stress: dependence on heat shock proteins. FEBS Lett 1999;461(3):306–10.
[2] Elrobh MS, Alanazi MS, Khan W, Abduljaleel Z, Al-Amri A, Bazzi MD. Molecular cloning and characterization of cDNA encoding a putative stress-induced heat-shock protein from Camelus dromedarius. Int J Mol Sci. 2011;12(7):4214–36.
[3] Mounier N, Arrigo AP. Actin cytoskeleton and small heat shock proteins: how do they interact?. Cell Stress Chaperones 2002;7(2):167–76.
[4] Willmer P, Stone G, Johnson I. Environmental Physiology of Animals, Chapter 14: Extreme terrestrial habbitats, pp532-536. Blackwell Science Ltd, Oxford. 1999.
[5] Grigg G, Beard L, Dorges B, Heucke J, Coventry J, Coppock A, et al. Strategic (adaptive) hypothermia in bull dromedary camels during rut; could it increase reproductive success?. Biol Lett 2009;5(6):853–6.
[6] Wu H, Guang X, Al-Fageeh MB, Cao J, Pan S, Zhou H, et al. Camelid genomes reveal evolution and adaptation to desert environments. Nat Commun 2014;5:5188.
[7] Velichko AK, Petrova NV, Razin SV, Kantidze OL. Mechanism of heat stress-induced cellular senescence elucidates the exclusive vulnerability of early S-phase cells to mild genotoxic stress. Nucleic Acids Res 2015;43(13):6309–20.
[8] Laszlo A, Venetianer A. Heat Resistance in Mammalian Cells: Lessons and Challengesa. Ann N Y Acad Sci. 1998;851(1 STRESS OF LIF):169-78.
[9] Zhang Y, Zhao H, Liu T, Wan C, Liu X, Gao Z, et al. Activation of transcription factor AP-1 in response to thermal injury in rat small intestine and IEC-6 cells. BMC Gastroenterol 2015;15(1):83.
[10] Saadeldin IM, Swelum AA-A, Elsafadi M, Mahmood A, Alfayez M, Alowaimer AN. Differences between the tolerance of camel oocytes and cumulus cells to acute and chronic hyperthermia. J Thermal Biol 2018;74:47–54.
[11] Tang HM, Tang HL. Cell recovery by reversal of ferroptosis. Biol Open 2019;8 (6):bio043182.
[12] Tang HL, Tang HM, Mak KH, Hu S, Wang SS, Wong KM, et al. Cell survival, DNA damage, and oncogenic transformation after a transient and reversible apoptotic response. Mol Biol Cell. 2012;23(12):2240–52.
[13] Saadeldin IM, Swelum AA-A, Noreldin AE, Tukur HA, Abdelazim AM, Abomughaid MM, et al. Isolation and culture of skin-derived differentiated and stem-like cells obtained from the Arabian camel (Camelus dromedarius). Animals 2019;9(6):378.
[14] Diaz FJ, Wigglesworth K, Eppig JJ. Oocytes determine cumulus cell lineage in mouse ovarian follicles. J Cell Sci 2007;120(8):1330–40.
[15] Mestdagh P, Feys T, Bernard N, Guenther S, Chen C, Speleman F, et al. High-throughput stem-loop RT-qPCR miRNA expression profiling using minute amounts of input RNA. Nucleic Acids Res 2008;36(21):e143-e.
[16] Magdeldin S, Yamamoto T, Tooyama I, Abdelalim EM. New proteomic insights on the role of NPR-A in regulating self-renewal of embryonic stem cells. Stem Cell Rev 2014;10(4):561–72.
[17] Gokce E, Shuford CM, Franck WL, Dean RA, Muddiman DC. Evaluation of normalization methods on GeLC-MS/MS label-free spectral counting data to correct for variation during proteomic workflows. J Am Soc Mass Spectro 2011;22(12):2199–208.
[18] Magdeldin S, Yamamoto K, Yoshida Y, Xu B, Zhang Y, Fujinaka H, et al. Deep proteome mapping of mouse kidney based on OFFGel prefractionation reveals remarkable protein post- translational modifications. J Proteome Res 2014;13 (3):1636–46.
[19] Vizcaino JA, Csordas A, del-Toro N, Dianes JA, Griss J, Lavidas I, et al. 2016 update of the PRIDE database and its related tools. Nucleic Acids Res. 2016;44 (D1):D447-56.
[20] MacLean-Fletcher S, Pollard TD. Mechanism of action of cytochalasin B on actin. Cell 1980;20(2):329–41.
[21] Xiang W, Rensing L. Changes in cell morphology and actin organization during heat shock in Dictyostelium discoideum: does HSP70 play a role in acquired thermotolerance?. FEMS Microbiol Lett 1999;178(1):95–107.
[22] Hong H, Kohli K, Garabedian MJ, Stallcup MR. GRIP1, a transcriptional coactivator for the AF-2 transactivation domain of steroid, thyroid, retinoid, and vitamin D receptors. Mol Cell Biol 1997;17(5):2735–44.
[23] Merret R, Nagarajan VK, Carpentier MC, Park S, Favory JJ, Descombin J, et al. Heat-induced ribosome pausing triggers mRNA co-translational decay in Arabidopsis thaliana. Nucleic Acids Res 2015;43(8):4121–32.
[24] Hong F, Mohammad Rachidi S, Lundgren D, Han D, Huang X, Zhao H, et al. Mapping the interactome of a major mammalian endoplasmic reticulum heat shock protein 90. PLoS ONE 2017;12(1):e0169260.
[25] Stevenson AF, Lange CS. Extracellular matrix (ECM) and cytoskeletal modulation of cellular radiosensitivity. Acta Oncol 1997;36(6):599–606.
[26] Zhang X, Li C, Gao H, Nabeka H, Shimokawa T, Wakisaka H, et al. Rho kinase inhibitors stimulate the migration of human cultured osteoblastic cells by regulating actomyosin activity. Cell Mol Biol Lett 2011;16(2):279–95.
[27] Amano M, Nakayama M, Kaibuchi K. Rho-kinase/ROCK: a key regulator of the cytoskeleton and cell polarity. Cytoskeleton (Hoboken) 2010;67(9):545–54.
[28] Ramachandran C, Patil RV, Combrink K, Sharif NA, Srinivas SP. Rho-Rho kinase pathway in the actomyosin contraction and cell-matrix adhesion in immortalized human trabecular meshwork cells. Mol Vis 2011;17:1877–90.
[29] Sadian Y, Gatsogiannis C, Patasi C, Hofnagel O, Goody RS, Farkasovsky M, et al. The role of Cdc42 and Gic1 in the regulation of septin filament formation and dissociation. Elife 2013;2:e01085.
[30] Schwartz M. Rho signalling at a glance. J Cell Sci 2004;117(Pt 23):5457–8.
[31] Lodish H, Berk A, Kaiser CA, Krieger M, Bretscher A, Ploegh H, et al. Molecular Cell Biology, Eighth Edition, W. H. Freeman and Company, Macmillan Learning, New York. 2016.
[32] Flanders KC, Winokur TS, Holder MG, Sporn MB. Hyperthermia induces expression of transforming growth factor-beta s in rat cardiac cells in vitro and in vivo. J Clin Invest 1993;92(1):404–10.
[33] Elsafadi M, Manikandan M, Dawud RA, Alajez NM, Hamam R, Alfayez M, et al. Transgelin is a TGFβ-inducible gene that regulates osteoblastic and adipogenic differentiation of human skeletal stem cells through actin cytoskeleston organization. Cell Death Dis 2016;7(8)::e2321-e.
[34] Inman GJ, Nicolas FJ, Callahan JF, Harling JD, Gaster LM, Reith AD, et al. SB-431542 is a potent and specific inhibitor of transforming growth factor-beta superfamily type I activin receptor-like kinase (ALK) receptors ALK4, ALK5, and ALK7. Mol Pharmacol 2002;62(1):65–74.
[35] Cai H, Ren Y, Li XX, Yang JL, Zhang CP, Chen M, et al. Scrotal heat stress causes a transient alteration in tight junctions and induction of TGF-β expression. Int J Androl 2011;34(4pt1):352–62.
[36] Wang S-H, Cheng C-Y, Tang P-C, Chen C-F, Chen H-H, Lee Y-P, et al. Differential gene expressions in testes of L2 strain Taiwan country chicken in response to acute heat stress. Theriogenology 2013;79(2). 374 82.e7.
[37] He S, Hou X, Xu X, Wan C, Yin P, Liu X, et al. Quantitative proteomic analysis reveals heat stress-induced injury in rat small intestine via activation of the MAPK and NF-κB signaling pathways. Mol BioSyst 2015;11(3):826–34.
[38] Johannes L, Jacob R, Leffler H. Galectins at a glance. J Cell Sci 2018;131(9).
[39] Pompella A, Visvikis A, Paolicchi A, De Tata V, Casini AF. The changing faces of glutathione, a cellular protagonist. Biochem Pharmacol 2003;66(8):1499–503.
[40] Kumar C, Igbaria A, D'Autreaux B, Planson A-G, Junot C, Godat E, et al. Glutathione revisited: a vital function in iron metabolism and ancillary role in thiol-redox control. EMBO J 2011;30(10):2044–56.
[41] Bustin SA, Benes V, Garson JA, Hellemans J, Huggett J, Kubista M, et al. The MIQE guidelines: minimum information for publication of quantitative real-time PCR experiments. Clin Chem 2009;55(4):611–22.
[42] Wei Y, Chiang WC, Sumpter Jr R, Mishra P, Levine B. Prohibitin 2 is an inner mitochondrial membrane mitophagy receptor. Cell 2017;168(1-2). 224-38 e10.
[43] Lüders J, Demand J, Höhfeld J. The ubiquitin-related BAG-1 provides a link between the molecular chaperones Hsc70/Hsp70 and the proteasome. J Biol Chem 2000;275(7):4613–7.
[44] Richter K, Haslbeck M, Buchner J. The heat shock response: life on the verge of death. Mol Cell 2010;40(2):253–66.
[45] Tang HM, Talbot Jr CC, Fung MC, Tang HL. Molecular signature of anastasis for reversal of apoptosis. F1000. Research 2017;6:43.
[46] Beere HM, Wolf BB, Cain K, Mosser DD, Mahboubi A, Kuwana T, et al. Heat-shock protein 70 inhibits apoptosis by preventing recruitment of procaspase-9 to the Apaf-1 apoptosome. Nat Cell Biol 2000;2(8):469–75.
[47] Guo S, Wharton W, Moseley P, Shi H. Heat shock protein 70 regulates cellular redox status by modulating glutathione-related enzyme activities. Cell Stress Chaperon 2007;12(3):245–54.
[48] Babady NE, Pang YP, Elpeleg O, Isaya G. Cryptic proteolytic activity of dihydrolipoamide dehydrogenase. Proc Natl Acad Sci USA 2007;104 (15):6158–63.
[49] Sun J, Mu H, Zhang H, Chandramouli KH, Qian P-Y, Wong CKC, et al. Understanding the regulation of estivation in a freshwater snail through iTRAQ-based comparative proteomics. J Proteome Res 2013;12(11):5271–80.
[50] Barber RD, Harmer DW, Coleman RA, Clark BJ. GAPDH as a housekeeping gene: analysis of GAPDH mRNA expression in a panel of 72 human tissues. Physiol Genom 2005;21(3):389–95.
[51] Coutry N, Farman N, Bonvalet JP, Blot-Chabaud M. Role of cell volume variations in Na(+)-K(+)-ATPase recruitment and/or activation in cortical collecting duct. Am J Physiol 1994;266(5 Pt 1):C1342–9.
[52] Gong YN, Crawford JC, Heckmann BL, Green DR. To the edge of cell death and back. FEBS J 2019;286(3):430–40.
[53] Raj AT, Kheur S, Bhonde R, Gupta AA, Patil VR, Kharat A. Potential role of anastasis in cancer initiation and progression. Apoptosis 2019;24(5–6):383–4.